Journal of the Korean Society of Marine Environment & Safety
Research Paper
Vol. 25, No. 1, pp. 130-137, February 28, 2019, ISSN 1229-3431(Print) / ISSN 2287-3341(Online) https://doi.org/10.7837/kosomes.2019.25.1.130

Numerical Analysis on the Cavitation Performance of a Seawater Cooling Pump

Bao Ngoc Tran* · Jun-ho Kim**†
* Graduate School of Mokpo National Maritime University, Mokpo 58628, Korea
** Division of Mechatronics Engineering, Mokpo National Maritime University, Mokpo 58628, Korea

해수냉각 펌프의 캐비테이션 성능에 대한 수치해석

Bao Ngoc Tran* · 김준호**†
* 목포해양대학교 대학원, ** 목포해양대학교 해양메카트로닉스학부

Abstract : *In this study, a centrifugal seawater cooling pump was analyzed to investigate its cavitation behavior over different operating flow rates. 3D two-phase simulations were carried out with ANSYS-CFX commercial code. The k-ε turbulence and Rayleigh-Plesset cavitation models were employed in the simulations. A head drop characteristics curves for three discharge rates was built based on numerical predictions. At higher flow rates, the impeller was more vulnerable to bubble cavitation. The 3 % head drop points of the pump working at 0.7Q, Q, and 1.3Q (Q: design flow rate) corresponded with NPSHa 1.21 m, 1.83 m, and 3.45 m, respectively. The volume of vapor bubbles was estimated and cavitation locations were anticipated to visualize the development of the cavity within the impeller. Moreover, the distribution of pressure coefficient and a blade loading chart are specifically presented, bringing out the harmful impacts of cavitation on the pump operation.*

Key Words : *CFD, Cavitation, Bubble formation, Centrifugal pump, NPSHa*

요 약 : 원심 해수냉각 펌프를 분석하기 위하여 다른 운전 유량에 대한 캐비테이션 거동을 조사하였다. 3D 2상 해석은 ANSYS-CFX 상용코드로 수행되었다. 해석에는 *k-ε* 난류와 *Rayleigh-Plesset cavitation* 모델이 사용되었다. 수치 예측에 기초하여 세 가지 토출 유량값에 대하여 헤드 드롭 특성곡선이 작성되었다. 더 높은 유량에서 임펠러는 버블 캐비테이션에 보다 취약하다. 0.7Q, Q 및 1.3Q(Q: 설계 유량)에서 작동하는 펌프의 3 % 헤드 드롭 위치는 각각 NPSHa 1.21 m, 1.83 m 및 3.45 m에 해당한다. 증기 기포의 볼륨이 예측되고 캐비테이션의 위치는 임펠러 내에서 발생하는 캐비티를 시각화하여 예상하였다. 또한, 압력계수와 날개 부하 분포가 구체적으로 제시되어 캐비테이션이 펌프 운전에 미치는 해로운 영향을 나타냈다. 또한, 압력계수 분포와 날개부하 차트가 구체적으로 제시되어, 펌프 운전에 캐비테이션이 미치는 해로운 영향을 나타냈다.

핵심용어 : 전산유체역학, 캐비테이션, 기포 형성, 원심펌프, 유효흡입수두

1. Introduction

Centrifugal pumps are one of the most common types of turbo-machinery which are widely employed in a vast amount of applications. By converting the rotational kinetic energy to the hydrodynamic energy of the fluid flow, centrifugal pumps are used to transport fluid or raise its pressure. Although this type of pump is well-known for high reliability, centrifugal pumps may suffer from several risks of damage during the operating period and cavitation is one of the most detrimental phenomenon. Cavitation is defined as the formation of the vapor bubble at the regions where liquid pressure falls below the vapor pressure. At higher pressure areas, the bubble suddenly collapses and generates intense shock waves which lead to serious damage on the surface of metal components as well as degrade pump head and efficiency. Therefore it is significantly harmful to centrifugal pumps performance.

A great effort has been made by researchers in the field of

* First Author : ngoctranbao.hn@gmail.com, 061-240-7472
† Corresponding Author : junho.kim@mmu.ac.kr, 061-240-7241

cavitation analysis. There are plenty of literature denoted the adverse effects of cavitation and prediction methods applied in centrifugal pumps. Nohmi employed two CFD codes, namely STAR-CD with a locally homogeneous model of two-phase medium (TE model) and CFX-TASCflow with Constant enthalpy vaporization model (CEV model) to compute cavitation flow in a low specific speed centrifugal pump (Nohmi et al., 2003). The computational results showed that the former can predict gradual head drop but unstable while the later cannot do the same thing and needs more improvement. The unsteady cavitation at the tongue of the pump volute was captured and analyzed (Bachert et al., 2010) by means of PIV measurement to explain the reason for 3 % head drop when the pump operates at the excess flow rate. The authors found that at NPSH 3 %, almost no cavitation appears on the impeller blade while the tongue of spiral casing witnesses cavity violently. Stuparu (Stuparu et al., 2011) presented a new method for determination for the cavitation inception coefficient and cavitation behavior of a large centrifugal pump. By using CFD method combined with experiments, Zhu (Zhu et al., 2014) investigated the cavitating characteristics in a centrifugal pump with gap impeller. It is reported that impeller with gap structure at leading edge has a superior feature of cavitation suppression. A relative accurate respond model based on computational simulations and Radial Basic Function was built by Zhang in order to predict the effect of the shape of blade leading edges on the cavitation performance of a centrifugal pump (Zhang et al., 2016).

The present study emphasizes a centrifugal seawater cooling pump used on board a training ship. Its function is to convey and circulate seawater in a cooling system. The main engine and auxiliary machinery generate heat in the combustion process during their operation. These amount of heat need to be transferred to cooling water to ensure those machines function properly within a safe range of operating temperature. Therefore, the research on seawater cooling pump's cavitation behavior plays an essential role in marine safety operation. Cavitation results in not only the reduction in pump performance and efficiency but also physical damage, vibration, and noise (Cernectic and Cudina, 2011). In this pump, the cavitation phenomenon is anticipated by means of CFD technic. The advance CFX commercial code enables a prediction of the cavitation evolution within pump impeller as suction pressure reduces. Based on that the head-drop characteristics curves at different flow rate are built to indicate the moment NPSH 3% occurs. Besides, the visualization of cavity position, volume fraction of vapor bubbles as well as the loading on the blade at various cavity levels are well illustrated.

2. Pump specification

2.1 Pump specification

A seven-blade centrifugal pump used in the seawater cooling system is chosen to carry out the research. The pump's components are displayed in Fig. 1, including a close type impeller, a curved intake section, and a spiral volute casing. The intake section is equipped with a swirl breaker to mitigate the harmful effect of the vortex on the flow before water enters the impeller. The impeller's inner and outer diameter are $d_1 = 60$ mm and $d_2 = 284$ mm in turn. It is designed to operate at a rotational speed of 1780 rpm, corresponding to a specific $N_s = 685$ (metric unit). The flow escaped the impeller is discharged into a spiral volute casing with a mean circle diameter $d_3 = 297$ mm. At the best efficiency point (BEP), the designed flow rate is 140 m^3/h and the designed head is 41m. The side chamber clearance between impeller and casing is also included to take the effect of leakage flow into account. The pump's parameters are summarized in Table 1.

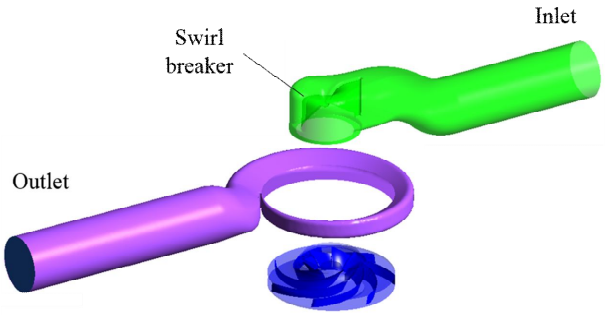

Fig. 1. Pump geometry.

Table 1. Pump design parameters

Parameter	Sign	Value	Unit
Head	H	41	m
Rotational speed	N	1780	RPM
Inlet diameter of impeller	d_1	60	mm
Outlet diameter of impeller	d_2	284	mm
Number of blades	Z	7	-
Outlet blade angle	β_2	28	deg
Outlet width of impeller	b_2	20	mm
Clearance at impeller wear ring	cl	0.25	mm
Diameter of cut-water	d_3	297	mm
Suction and discharge pipe diameter	ϕ	125	mm

2.2 Mesh strategy

The whole fluid domains of the pump are meshed using Mesh module in ANSYS Workbench based on unstructured tetrahedra elements. Three main components, including suction domain, impeller domain, and volute domain are built and meshed independently. The mesh at leading edges of impeller blades is refined and an inflation of 10 layers is applied to all wall surfaces in order to increase the accuracy of calculations for the flow at near wall areas.

Theoretically, the finer the mesh is, the fewer grid-related errors are (Ferziger and Peric, 1996). Therefore, a sensibility analysis is conducted to ensure the independence of simulation results with respect to the grid size. In this analyze, non-cavitation model is utilized and the head coefficient at design point is chosen as a standard parameter to evaluate grid size effect (Tran et al., 2017). The final grid consisted of 4.9 million elements, where the size of the suction domain, impeller domain, and volute domain were 1.1 million, 2.6 million, and 1.2 million elements respectively. This size of the grid was considered to guarantee for both grid independence and the calculations time. The mesh parameters are provided in Table 2 and the mesh formation is displayed in Fig. 2.

Table 2. Mesh parameters

Mesh Parameters		Value
Type of mesh		Unstructured
Number of Elements	Suction	1.1 million
	Impeller	2.6 million
	Volute	1.2 million
	Total	4.9 million

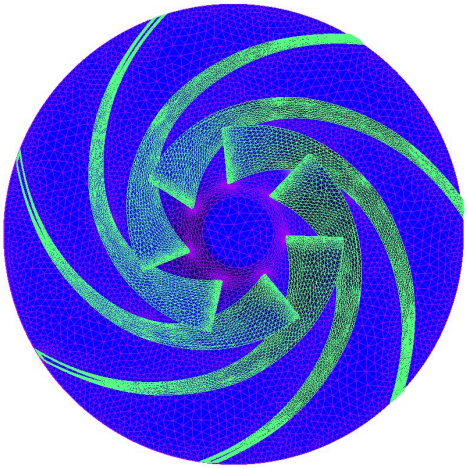

Fig. 2. Refined mesh the of the impeller.

3. Numerical method

3.1 Turbulence model

In this numerical analysis, a commercial CFD code - CFX is employed to investigate the cavitation phenomenon within the impeller of the centrifugal pump. It is a multi-purpose CFD code to solve three dimensional Reynolds Average Navier-Stock (RANS) equation for steady and turbulent fluid flow. The validation of CFX can be found in several researches on pumps cavitation done by Lorusso (Lorusso et al., 2017), Kim (Kim et al., 2012), and Caridad (Caridad et al., 2008).

Based on the results reported by Tran (Tran et al., 2015), k - ε turbulence model coupled with and Rayleigh-Plesset cavitation model gave the numerical results closer to experimental data than Shear Stress Transport turbulence model. Therefore, the k - ε turbulence model with log-law wall function is applied in simulations.

3.2 Cavitation model

The Rayleigh-Plesset cavitation model governing the dynamics of spherical bubbles in an incompressible fluid is used in this research to simulate and visualize the formation of cavitation. The Rayleigh-Plesset equation describing the growth of the vapor bubbles is as follows:

$$R_B\frac{d^2R_B}{dt^2}+\frac{3}{2}\left(\frac{dR_B}{dt}\right)^2+\frac{2\sigma}{\rho R_B}=\frac{P_v-P}{\rho} \quad (1)$$

where, R_B is the bubble radius, P_v is the pressure in the bubble, P is the pressure in the liquid surrounding the bubble, σ is the surface tension coefficient, ρ is the liquid density.

The liquid water at 25°C and vapor water at 25°C are working fluid in two-phase cavitation simulations. The average diameter of vapor bubble is set as 2.10^{-6} m while saturated vapor pressure is 3574 Pa. At first, the simulation of fluid flow with non-cavitation model is carried out. Then it is employed as an initial value for cavitation flow simulations by decreasing step by step the suction pressure at the inlet of the pump. Along with the reduction in suction pressure, the Net Positive Suction Head (NPSH) also drops gradually. NPSH is the different head between the pressure at the inlet and vapor pressure of the liquid, and is given as Equation 2:

$$NPSH=\frac{P_{Suction}-P_{Vapor}}{g\cdot\rho} \quad (2)$$

where $P_{Suction}$ is the pressure at the inlet [Pa], P_{Vapor} is the vapor pressure of the fluid [Pa].

The Pressure coefficient is calculated by Equation 3:

$$C_p = \frac{P_{Local} - P_{Suction}}{g.\rho.H} \quad (3)$$

where P_{Local} is the pressure at local position [Pa], H is the pump head [m].

3.3 Boundary condition

Concerning to the calculation domains, the extensions of 2D at suction domain and 3D at volute-discharge domain are implemented for numerical and physical reasons. Thank to that some of the convergence problems and related flow instabilities can be prevented. In numerical simulations, multiple frames of reference are involved. The suction and discharge domains are set as stationary frame meanwhile impeller domain is a type of rotational frame. The interfaces between two stationary domains are set as general connection while those between rotational and stationary components are set as frozen-rotor type. The rotating and stationary frame are connected in such a manner that the relative position of impeller and volute domain is constant by the time in steady state analysis. The conveyance critical of the simulations is set as 10^{-5}.

In order to characterize the cavitation phenomenon, the present study is conducted with the following boundary conditions put into set up:

At the inlet of the suction domain, a total pressure is set, and then the suction pressure reduces little by little to facilitate the formation of the vapor bubbles. The volume fraction of liquid water is 1 and volume fraction of vapor water is 0. The turbulent intensity is specified as 5 %.

As for the outlet, three values of mass flow rates including $0.7Q_{design}$, Q_{design} and $1.3Q_{design}$ are applied. Rough wall condition is imposed on all the wall of every domain with a value of 0.01 mm.

4. Results and discussion

4.1 Pump performance in single phase analysis

At first, in order to verify the accuracy of numerical method and create initial conditions for cavitation analysis, we carry out the simulations on the pump performance in single phase. In these simulations, the cavitation model is turn off and sole liquid water is employed as a working fluid. The head coefficient, flow coefficient, and efficiency of the pump are calculated by equations below:

$$\Psi = \frac{gH}{\omega^2 D^2} \quad (4)$$

$$\Phi = \frac{Q}{\omega D^3} \quad (5)$$

$$\eta = \frac{g\rho QH}{T.\omega} \quad (6)$$

where Ψ is the head coefficient, Φ is the flow coefficient, η is the pump efficiency, H is the pump head [m], ω is the rotational speed [Rad/s], D is the impeller outer diameter [m], Q is the flow rate [m^3/s], T is the torque on the pump shaft [N.m].

The head - flow coefficient curve and efficiency - flow coefficient curve of the pump are plotted in Fig. 3. Two characteristics are investigated in a wide range of flow rate, from 0.4 to 1.4 times of designed flow rate. The numerical simulations with the flow rate out of above range is not conducted because the results are not reliable due to convergence problems caused by large recirculation within the volute casing and impeller passages at excess discharge rate and the over prediction of loss by the numerical computation at lower flow rate.

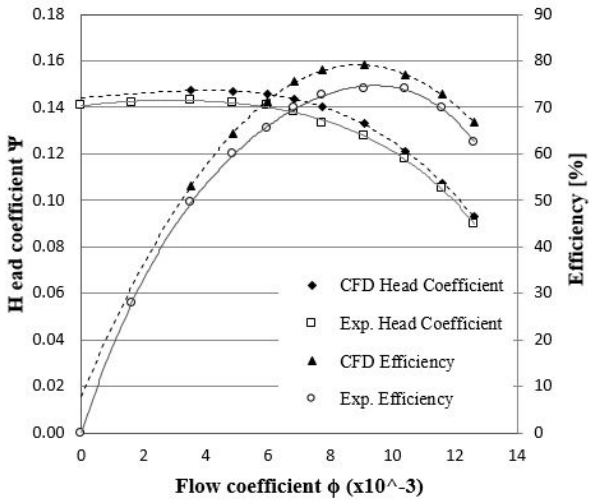

Fig. 3. Pump head and efficiency in single phase analysis.

In general, the head coefficient and efficiency of simulation results follow the same trend as experimental data. Two

performance curves anticipated by CFD method show a good agreement with experimental curves. In cases of head coefficient, at the best efficiency point (BEP) corresponding to flow coefficient 8.9×10^{-3} the numerical predicted Ψ is 0.1330 in comparison with experimental data Ψ of 0.1278, making a disparity of 4.1 %. With the raise of flow coefficient, the gap between experimental and calculated head coefficient is become smaller.

In terms of the efficiency curve, the numerically estimated efficiency witnesses a difference of 5 % between numerical and experimental data at the designed flow rate, 79% and 74% respectively. Reasons for above discrepancies are other types of head loss in actual operating condition. In the simulations, the volumetric head loss at the wearing and the friction head loss at the component's wall are involved. Nevertheless, there are some other types of loss needed to be included in centrifugal pump performance prediction. If so, a better agreement between simulation and experiment is likely to achieve.

4.2 Pump cavitation performance curves

The pump cavitation behavior is investigated by applying the cavitation model at different flow rate values. For each flow rate, the non-cavitation simulation result is utilized as an initial condition, hence the suction pressure is reduced progressively. The reduction of suction pressure gives raise for the fall of Net Positive Suction Head available (NPSHa). When the NPSHa drops to a certain value, low-pressure areas appear and the formation of vapor bubbles begins. Fig. 4 shows the relationship between the pump head and NPSHa at three values of flow rate, namely 98 m^3/h, 140 m^3/h, and 195 m^3/h corresponding to 0.7Q, Q, and 1.3Q in turn (Q is the design flow rate).

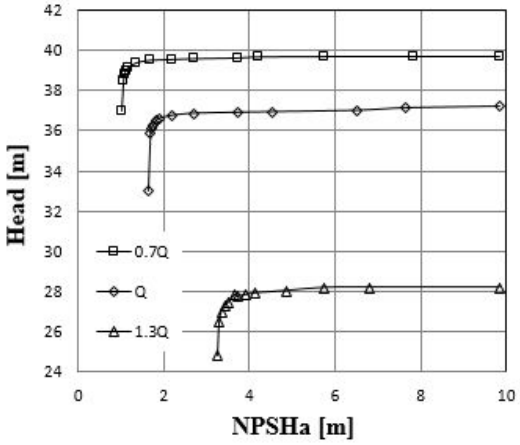

Fig. 4. Head - NPSH drop curve at different flow rate.

As can be seen, the NPSHa with respect to cavity point of 0.7Q is the smallest, followed by designed Q and 1.3Q. Based on the numerical predictions, the NPSHa at which the pump head suddenly drops are 1.02 m, 1.63 m, and 3.26 m for 0.7Q, Q, and 1.3Q respectively. That means with the same NPSHa (the same suction head) the pump operating at excess flow rate is likely to suffer from head drop by cavitation than at lower flow rate.

The point of NPSHa where cavitation makes a head drop of 3 % compared to initial pump head is called NPSH 3 %. Beyond this point, the cavitation is accused seriously harmful to the pump operation. The alteration of NPSH 3 % with the flow rate is displayed in Fig. 5. A higher flow rate results on the higher value of NPSH 3 %. The NPSH 3 % goes up gradually from 1.1 m (for 0.5Q) to 1.8 m (for Q) and rockets up to 3.4 m (for 1.3Q). NPSH 3 % is also considered as a critical value that NPSHa must be higher to ensure the normal operation of the pump with negligible effect of cavitation.

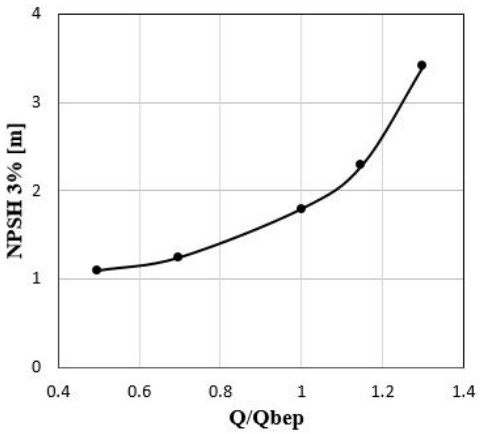

Fig. 5. Variation of NPSH 3 % with flow rate.

4.3 Evolution and effect of cavitation

The volume of bubbles created by vapor water inside the pump is an important factor to determine the degree of cavitation. Fig. 6 demonstrates the volume of the vapor water within the impeller at the same NPSHa = 2.67 at different flow rate. The most significant feature observed from the chart is that the volume of bubbles increases along with the reduction of vapor water volume fraction and at a similar suction pressure the 1.3Q-case generates the quantity of vapor bubble much more than two remaining cases. Meanwhile, the volume of vapor water at designed Q is double that one at 0.7Q in most of the plotted volume fraction value.

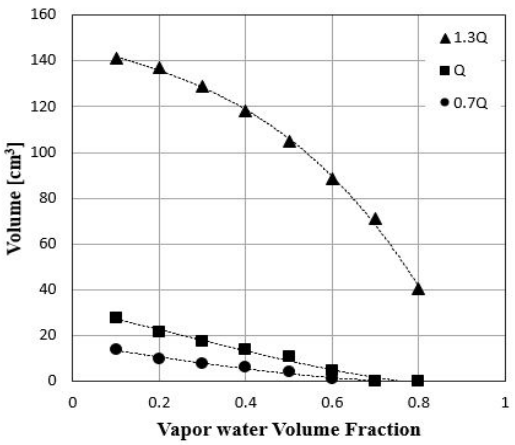

Fig. 6. Volume of vapor water at NPSHa = 2.67.

The higher volume of bubbles, the more seriously cavitation occurs. Due to the centrifugal force of rotating impeller, those bubbles move from low-pressure areas to high-pressure areas. They collapse rapidly and generate shock wave attacking metal surfaces which is the source of vibration, noise, and erosion. Moreover, in the case of 1.3Q, the huge number of vapor bubbles takes much space of liquid water, choking the impeller passages. It results in a sudden drop of the pump head and a poor performance under grave cavitation.

In order to visualize the cavitation phenomenon, the distribution of vapor water on the impeller hub and blade is illustrated in Fig. 7. The volume fraction of vapor water ranges from 0 to 1 where 0 means no vapor gas and 1 means full of vapor gas. It is clear that at NPSHa = 2.67 the location of bubbles on impeller blades are widened along with the rise of flow rate. The formation of vapor bubbles firstly begins at the suction side, leading edge of the blades. Afterward, it extends progressively toward the trailing edge alongside the blade length. In case of low suction pressure corresponding to NPSHa = 2.67, the areas and level of bubbles formation at 0.7Q is the smallest, followed by Q with a slightly larger while that area at 1.3Q is the largest. When the pump operates at excess discharge rate the bubbles not only locates at the suction side but also further develops at the pressure side of the blade. It indicates that the flow channels between blades are seriously blocked by a number of bubbles and the pump is no longer able to continuously supply the liquid water with sufficient head.

The pressure coefficient (C_p) is a dimensionless number which describes the relative pressure throughout the flow field. Relying on this factor, low-pressure regions which are sensitive to cavity can be determined and cavitation locations are able to be predicted. The pressure coefficient is calculated by Equation 6, its distribution on the suction and pressure side of the impeller blades at designed flow rate is well captured and illustrated in Fig. 8. It is notable that the areas with low C_p located in leading edge, suction side of the blade where the pressure is lower than other regions. These vulnerable positions are likely to suffer from bubbles formation. That feature is reasonable to the results observed from Fig. 7.

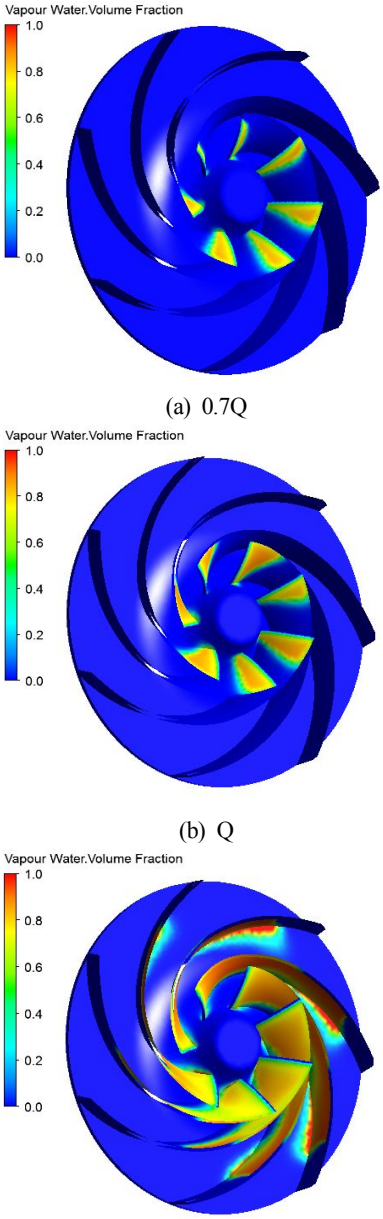

(a) 0.7Q

(b) Q

(c) 1.3Q

Fig. 7. Volume fraction of vapor water on the impeller (NPSHa = 2.67).

Meanwhile, C_p value increases step by step alongside the meridional length of the blade, reaching a value of 0.8 at the regions near trailing edge. The comparison of C_p arrangement between several NPSH values reveals that according to the decrease of NPSHa the low-C_p zone extent downstream from leading edge to the blade trailing edge. In case of NPSHa = 1.66, the area of -0.1C_p is 5 times larger than that area for NPSHa = 9.83 and it further develops when NPSHa drops to 1.16. In the final circumstance, the low-C_p region comprises for over a haft of blade both suction and pressure side, indicating a strong evolution of cavity and a sharp reduction in pump head due to obstruction at the throat.

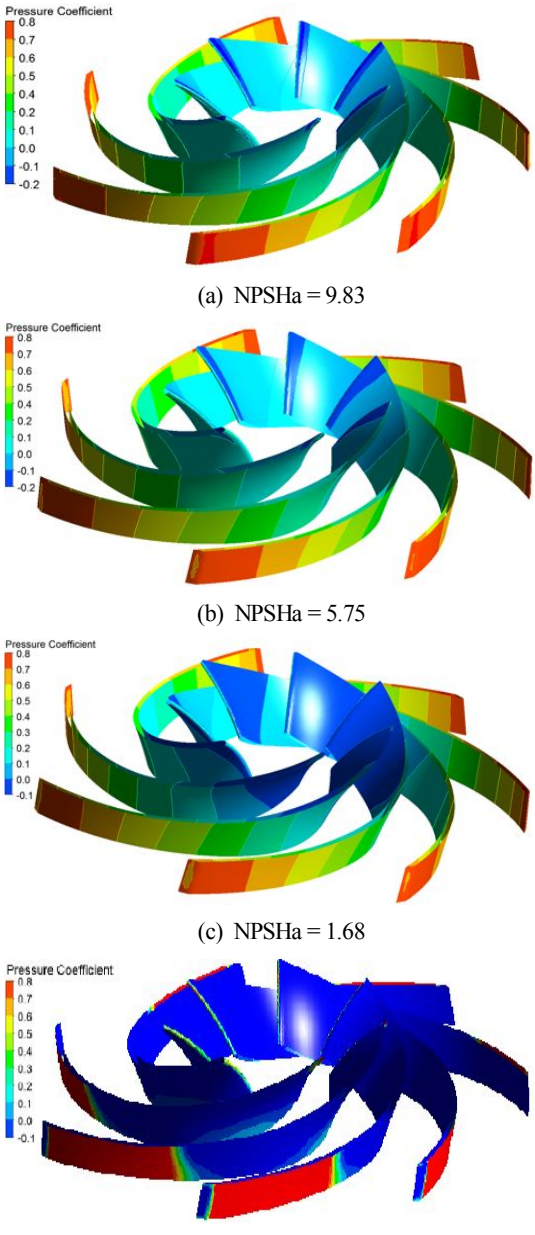

(a) NPSHa = 9.83

(b) NPSHa = 5.75

(c) NPSHa = 1.68

(d) NPSHa = 1.16

Fig. 8. Pressure Coefficient Cp distribution on blades at Q designed.

In this study, the impact of cavitation phenomenon on blade loading is also brought out by Fig. 9. The curves show the variation of the load acting on the blade in 4 cases of NPSHa and a case of single simulation where cavitation mode is turned off. At high NPSHa = 9.83, the load on the suction side and pressure side of the blade are almost same as blade loading in single phase analysis, showing that there is no cavitation as well as no vapor bubble at all. The fall of suction head gives raise for bubble formation which takes much space of liquid water and prevents the energy transfer process between impeller and liquid water. It explains the cause of static pressure on blade surface deteriorates at low values of NPSHa (5.75 and 1.68). The smallest NPSHa = 1.16 witnesses a collapse of blade loading. There is no load on the blade within over a haft of the blade length, making the impeller unable to push the liquid. In this situation, the pump suffers from serious cavitation with a number of bubbles filled up the flow passages, performing bad behavior with extremely low efficiency. This tremendous reverse effect has been predicted and mentioned in Fig. 8.

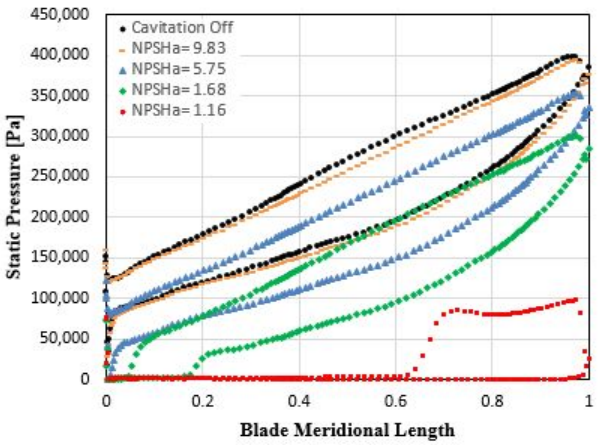

Fig. 9. Static pressure on the blade at various NPSHa.

5. Conclusion

This paper presents a numerical study on the cavitation prediction of a seawater cooling pump and focuses on the relationship between the flow rate and cavitation occurrence. The simulations in two-phase flow with Rayleigh-Plesset cavitation model are conducted to observed some key points as follows:

The advance CFD code has implemented a good prediction on the pump performance in both single-phase and two-phase flow analysis. Pump head coefficient curve, efficiency curve, and head-NPSH curve are built with less time and progress. A comparison between numerical results and experimental data given by manufacturer shows a small disparity, accounting for less than 5 %.

The evolution of bubbles formation is well captured and illustrated. A reduction on the suction pressure results in the existence of vapor bubbles in the regions near impeller crown and blade leading edge. The cavity firstly appears at the suction side then extends to the pressure side of the blade. At low NPSHa, a large amount of bubbles chock the passages, causing a remarkable head drop.

The risk of occurrence of cavitation at excess flow rate is higher than partial flow rate. At the same NPSHa, the volume of vapor water and cavitation level in the pump working at 1.3Q is more serious than working at Q and 0.7Q.

References

[1] Bachert, R., B. Stoffel and M. Dular(2010), Unsteady Cavitation at the Tongue of the Volute of a Centrifugal Pump, Journal of Fluids Engineering, Vol. 132, No. 6, pp. 061304-1-061301-6.

[2] Caridad, J., M. Asuaje, F. Kenyery, A. Tremante and O. Aguillon(2008) Characterization of a centrifugal pump impeller under two-phase flow conditions. Journal of Petroleum Science and Engineering, Vol. 63, pp. 18-22.

[3] Cernetic, J. and M. Cudina(2011), Estimating unsteady of measurements for cavitation detection in a centrifugal pump, Measurement, Vol. 44, No. 7, pp. 1293-1299.

[4] Ferziger, J. H. and M. Peric(1996), Computational Method of Fluid Dynamics, Springer, Berlin, Germany.

[5] Kim, M. J., H. B. Jin and W. J. Chung(2012), A Study on Prediction of Cavitation for centrifugal pump, International Journal of Mechanical, Vol. 6, No. 12, pp. 2720-2725.

[6] Lorusso, M., T. Capurso, M. Torresi, B. Fortunato, F. Fornarelli, S. M. Camporeale and R. Monteriso(2017), Efficient CFD evaluation of the NPSH for centrifugal pumps, Energy Procedia, Vol. 126, pp. 778-785.

[7] Nohmi, M., A. Goto, Y. Iga and T. Ikohagi(2003), Cavitation CFD in a centrifugal pump, Proceeding of Fifth International Symposium on Cavitation, pp. 1-7.

[8] Stuparu, A., R. S. Resiga, L. E. Anton and S. Muntean(2011), A New Approach in Numerical Assessment of the Cavitation Behaviour of Centrifugal Pumps, International Journal of Fluid Machinery and System, Vol. 4, No. 1, pp. 104-113.

[9] Tran, B. N., C. J. Yang, B. G. Kim and J. H. Kim(2017), Internal Flow Analysis of Seawater Cooling Pump using CFD, Journal of the Korean Society of Marine Environment and Safety, Vol. 23, No. 1, pp. 104-111.

[10] Tran, T. D., B. Nennemann, T. C. Vu and F. Guibault(2015), Investigation of Cavitation Models for Steady and Unsteady Cavitating Flow Simulation, International Journal of Fluid Machinery and Systems, Vol. 8, No. 4, pp. 240-253.

[11] Zhang, S., R. Zhang, S. Zhang and J. Yang(2016), Effect of Impeller Inlet Geometry on Cavitation Performance of Centrifugal Pumps Based on Radial Basis Function, International Journal of Rotating Machinery, Vol. 2016, pp. 1-9.

[12] Zhu, B., H. Chen and Q. Wei(2014), Numerical and Experimental Investigation of Cavitating Characteristics in Centrifugal Pumps with Gap Impeller, International Journal of Turno Jet-Engines, Vol. 31, No. 2, pp. 187-196.

Received : 2018. 12. 28.
Revised : 2019. 02. 22.
Accepted : 2019. 02. 25.